

A Posteriori Error Estimation for Multi-Stage Runge-Kutta IMEX Schemes

Jehanzeb H. Chaudhry¹, J.B. Collins², and John N. Shadid³

¹Department of Mathematics, The University of New Mexico,
Albuquerque, NM 87131

²Department of Mathematics, West Texas A&M University,
Canyon, TX 79016

³Computational Mathematics Department, Sandia National
Laboratories, Albuquerque, NM

April 24, 2022

Abstract

Implicit-Explicit (IMEX) schemes are widely used for time integration methods for approximating solutions to a large class of problems. In this work, we develop accurate *a posteriori* error estimates of a quantity of interest for approximations obtained from multi-stage IMEX schemes. This is done by first defining a finite element method that is nodally equivalent to an IMEX scheme, then using typical methods for adjoint-based error estimation. The use of a nodally equivalent finite element method allows a decomposition of the error into multiple components, each describing the effect of a different portion of the method on the total error in a quantity of interest.

1 Introduction

In this paper we consider *a posteriori* error analysis for multi-stage implicit-explicit (IMEX) schemes applied to autonomous nonlinear ODEs,

$$\begin{cases} \dot{y}(t) = f(y(t)) + g(y(t)), & t \in (0, T], \\ y(0) = y_0. \end{cases} \quad (1)$$

Here $y(t) \in \mathbb{R}^m$, $\dot{y} = dy/dt$ and $f, g : \mathbb{R}^m \rightarrow \mathbb{R}^m$. The right hand side of (1) is split such that g represents a much smaller time scale than f , and is often referred to as the “stiff” term. Systems of the form (1) often arise from spatial discretization of partial differential equations, such as, for example, convection-diffusion-reaction equations, and hyperbolic systems with relaxation [1], where

f represents the convection term and g represents the diffusion or relaxation term.

As opposed to *a priori* error bounds, *a posteriori* error estimates provide an accurate computation of the discretization error in a particular approximation. Accurate error estimation is a critical component of numerical simulations, being useful for reliability, uncertainty quantification and adaptive error control. In particular, we consider goal-oriented *a posteriori* error estimation. Often, the aim of a numerical simulation is to compute the value of a linear functional of the solution, a so called quantity-of-interest (QoI) defined as,

$$Q(y) \equiv (y(T), \psi), \quad (2)$$

where $\psi \in \mathbb{R}^m$ and (\cdot, \cdot) denotes the standard Euclidean inner product. In this paper we employ adjoint based *a posteriori* analysis to quantify error for a given QoI. Adjoint based error estimation is widely used for a host of numerical methods including finite elements, time integration, and multi-scale simulations [2, 3, 4, 5, 6, 7, 8, 9, 10, 11]. The error estimate weights computable residuals of the numerical solution with the solution of an adjoint problem to quantify the accumulation and propagation of error. Moreover, the estimate also identifies different contributions to the total error.

Developing accurate and stable time integration of systems of the form (1) is challenging as the term g represents time scales which are often order of magnitudes smaller than the time scales for the component f [12]. IMEX schemes are an important and widely used class of time integration methods for such evolutionary equations [13]. These schemes treat the f component explicitly while treating the g component implicitly. Hence, such schemes attempt to minimize the computational cost by balancing the number of nonlinear solves needed for an implicit scheme with the small time step required to maintain stability with an explicit scheme.

IMEX schemes are widely used for time integration methods for approximating solutions to a large class of problems [12, 14, 15, 16, 17, 18, 19, 20, 21, 13, 22]. IMEX schemes may be divided into two classes: multi-step IMEX schemes and multi-stage Runge-Kutta IMEX schemes. Multi-step IMEX schemes are a generalization of multi-step schemes like Adams-Bashforth or backward differentiation formulas (BDF) and utilize solution values from previous time nodes to form the solution at the current time node. While multi-step IMEX schemes possess good properties for diffusion dominated equations, they are not ideal for hyperbolic systems due to lack of stability which necessitates extremely small time steps [13]. The multi-stage Runge-Kutta IMEX schemes possess superior stability properties and are often the numerical integrator of choice for problems which are not diffusion dominated.

Adjoint-based *a posteriori* error estimation is widely applied to finite element approximations, as a variational formulation is needed to compute the error, however, there is some recent work which considers finite difference methods. Explicit multi-stage and multi-step time integrators are considered in [11] and multi-step IMEX schemes were considered in [10]. Error estimates for the Lax-

Wendroff scheme were developed in [23] and certain Godunov methods were analyzed in [24, 25, 26].

In this paper, we derive *a posteriori* error estimates for the multi-stage Runge-Kutta IMEX schemes. To derive an estimate, we must first represent the scheme as a finite element method. This is done by developing a finite element method that is “nodally equivalent” to a certain IMEX scheme. A nodally equivalent finite element approximation agrees with the IMEX approximation at the discretization nodes, while still being defined on the entire temporal domain. The error representation formula is then derived using well defined methods. In addition, we break the error estimate into components representing different contribution to the error. In this way we are able to discuss the contribution of the implicit and explicit portions of the method to the total error in the quantity of interest.

The paper is organized as follows. In §2 we discuss the Runge-Kutta IMEX schemes and formulate an equivalent finite element method. This equivalence allows us to carry out *a posteriori* analysis in §3. Numerical examples arising from the discretization of partial differential equations are presented in §4.

2 Preliminaries and Equivalent Finite Element Method

In this section, we introduce some notation, then give a brief review of generic ν -stage IMEX Runge-Kutta schemes. For a more complete discussion see [1, 12, 13]. Generic continuous Galerkin finite element methods are introduced for solving (1), and then the idea of nodal equivalency is explained and the equivalent finite element method is derived. Finally, we show second order convergence of the finite element solution.

2.1 Notation and Generic IMEX Runge-Kutta Schemes

We begin with some notation. All approximations discussed are based on a discretization defined by the nodes

$$0 = t_0 < t_1 < \dots < t_n < \dots < t_N = T,$$

with time step $k_n = t_{n+1} - t_n$. The IMEX approximation at each node is denoted by $Y_n \approx y(t_n)$. Finally, for brevity we introduce notation for the subintervals $I_n := [t_n, t_{n+1}]$ and for sub-discretization nodes $t_{n+\tau} := t_n + k_n \tau$ with $\tau \leq 1$.

Multi-stage IMEX schemes are defined by two Butcher tableaus, one for the explicit method and another for the implicit method,

$$\begin{array}{c|c} \mathbf{c} & \mathbf{A} \\ \hline & \mathbf{w} \end{array} \quad \begin{array}{c|c} \mathbf{d} & \mathbf{B} \\ \hline & \mathbf{v} \end{array}, \quad (3)$$

where $A = (a_{ij}) \in \mathbb{R}^{\nu \times \nu}$ and $\mathbf{c}, \mathbf{w} \in \mathbb{R}^\nu$ define the explicit method and $B = (b_{ij}) \in \mathbb{R}^{\nu \times \nu}$ and $\mathbf{d}, \mathbf{v} \in \mathbb{R}^\nu$ define the implicit method. The update formula of

the IMEX scheme is given by,

$$\tilde{Y}_i = Y_n + k_n \sum_{j=1}^{i-1} a_{ij} f(\tilde{Y}_j) + k_n \sum_{j=1}^{\nu} b_{ij} g(\tilde{Y}_j), \quad (4)$$

$$Y_{n+1} = Y_n + k_n \sum_{i=1}^{\nu} w_i f(\tilde{Y}_i) + v_i g(\tilde{Y}_i). \quad (5)$$

Since the A matrix defines an explicit scheme, it must be strictly lower triangular. The implicit schemes we consider are DIRK schemes, therefore the matrix B is lower triangular. This condition ensures that $f(y)$ is always evaluated explicitly.

In this paper we examine three IMEX schemes in particular, Midpoint(1,2,2), IMEX-SSP3(3,3,2) and IMEX-SSP3(4,3,3). The names of these schemes are standardized and use a triplet notation (s, σ, p) where s is the number of stages in the implicit method, σ is the number of stages in the explicit method, and p is the order of the method as a whole. The Butcher tableaus for these schemes are shown in Tables 1, 2 and 3.

| | | | | | | |
|-----|-----|---|--|-----|---|-----|
| 0 | 0 | 0 | | 0 | 0 | 0 |
| 1/2 | 1/2 | 0 | | 1/2 | 0 | 1/2 |
| | 0 | 1 | | 0 | 1 | |

Table 1: Butcher Tableau for the explicit(left) and implicit(right) portion of the IMEX scheme Midpoint(1,2,2).

| | | | | | | | |
|-----|-----|-----|-----|------------|----------------|----------|----------|
| 0 | 0 | 0 | 0 | γ | γ | 0 | 0 |
| 1 | 1 | 0 | 0 | $1-\gamma$ | $1-2\gamma$ | γ | 0 |
| 1/2 | 1/4 | 1/4 | 0 | 1/2 | $1/2 - \gamma$ | 0 | γ |
| | 1/6 | 1/6 | 2/3 | | 1/6 | 1/6 | 2/3 |

Table 2: Butcher Tableau for the explicit(left) and implicit(right) portion of IMEX-SSP3(3,3,2). $\gamma = 1 - \frac{1}{\sqrt{2}}$

2.2 Finite Element Method

Adjoint-based error estimation requires that approximate solution must be defined for the entire domain $[0, T]$. This is done by using a finite element method to obtain the approximation. The same grid defined above is used to define the space of continuous piecewise polynomials,

$$\mathcal{C}^q = \{w \in C^0([0, T]; \mathbb{R}^m) : w|_{I_n} \in \mathcal{P}^q(I_n), 1 \leq n \leq N\}, \quad (6)$$

| | | | | | |
|----------|-----------|--------------|-------------------------------|----------|-----|
| | 0 | 0 | 0 | 0 | |
| | 0 | 0 | 0 | 0 | |
| | 1 | 0 | 1 | 0 | 0 |
| | 1/2 | 0 | 1/4 | 1/4 | 0 |
| | | 0 | 1/6 | 1/6 | 2/3 |
| α | α | 0 | | 0 | 0 |
| 0 | $-\alpha$ | α | | 0 | 0 |
| 1 | 0 | $1 - \alpha$ | | α | 0 |
| 1/2 | β | η | $1/2 - \beta - \eta - \alpha$ | α | |
| | 0 | 1/6 | | 1/6 | 2/3 |

Table 3: Butcher Tableau for the explicit(left) and implicit(right) portion of IMEX-SSP3(4,3,3). $\alpha = 0.24169426078821, \beta = 0.06042356519705, \eta = 0.12915286960590$

where $\mathcal{P}^q(I_n)$ is the space of all polynomials of degree q or less on I_n . The continuous Galerkin finite element method of order $q+1$ for (1), denoted cG(q), is defined interval-wise by,

Find $Y \in \mathcal{C}^q$ such that $Y(0) = y_0$ and for $n = 0, \dots, N-1$,

$$\langle \dot{Y}, v_n \rangle_{I_n} = \langle f(Y) + g(Y), v_n \rangle_{I_n}, \quad \forall v_n \in \mathcal{P}^{q-1}(I_n), \quad (7)$$

where $\langle \cdot, \cdot \rangle_{[a,b]} = \int_a^b (\cdot, \cdot) dt$ denotes the $L^2([a,b])$ inner product.

2.3 Equivalent Finite Element Method

In this section we construct a finite element method that is nodally equivalent to a particular IMEX scheme. Nodal equivalence was developed in [11] to compute error estimates for explicit Runge-Kutta and Adams-Bashforth schemes and in [10] for multi-step IMEX schemes. Two approximations are nodally equivalent if they are equal at the nodes t_n of the discretization. Two methods are nodally equivalent if they produce nodally equivalent approximations. Therefore the finite element approximation constructed in this section is a function $Y(t) \in \mathcal{C}^q$ with the property,

$$Y(t_n) = Y_n,$$

where Y_n is defined by one of the IMEX schemes discussed above.

We develop a nodally equivalent finite element method for the generic IMEX scheme defined by the Butcher tableaus (3). To obtain equivalency, we impose further conditions on these schemes by requiring all the elements of \mathbf{d} be distinct. The reason for this restriction is discussed below.

We begin by defining an approximation operator $\mathcal{I} : H^1([0, T]; \mathbb{R}^m) \rightarrow L^2([0, T]; \mathbb{R}^m)$. Denoting the restriction by $\mathcal{I}^n Y = \mathcal{I} Y|_{I_n}$, the operator is de-

finned by,

$$\mathcal{I}^n Y(t) = \sum_{i=1}^{\nu} \tilde{Y}_i \prod_{j=1, j \neq i}^{\nu} \frac{(t - t_{n+d_j})}{(t_{n+d_i} - t_{n+d_j})}. \quad (8)$$

where \tilde{Y}_i are the stage variables for the IMEX scheme. This operator approximates Y by interpolating through the stage variables from the IMEX scheme. Using this, the equivalent finite element method is defined by:

Find $Y \in \mathcal{C}^q$ such that $Y(0) = y_0$ and for $n = 0, \dots, N-1$,

$$\langle \dot{Y}, v_n \rangle_{I_n} = \langle f(\mathcal{I}Y), v_n \rangle_{I_n, Q^f} + \langle g(\mathcal{I}Y), v_n \rangle_{I_n, Q^g} \quad \forall v_n \in \mathcal{P}^{q-1}(I_n). \quad (9)$$

where the particular quadratures are defined by

$$\langle \varphi \rangle_{I_n, Q^f} = k_n \sum_{i=1}^{\nu} w_i \varphi(t_{n+d_i}), \quad (10)$$

$$\langle \varphi \rangle_{I_n, Q^g} = k_n \sum_{i=1}^{\nu} v_i \varphi(t_{n+d_i}). \quad (11)$$

Remark 1. We now see the reason for the condition that the elements of \mathbf{d} be distinct. If they were not distinct, then the definition of $\mathcal{I}^n Y$ would be ill-defined at t_{n+d_i} . It is possible to develop a nodally equivalent method without this restriction, but the definition would be considerably more complicated.

Now that we have the definition of a finite element method, we show that the resulting approximation is nodally equivalent to its corresponding IMEX scheme approximation.

Theorem 1. *The approximation $Y(t)$ obtained from the finite element method (9) is nodally equivalent to the approximation $\{Y_n\}$ obtained from the IMEX scheme defined by the Butcher tableaux (3).*

Proof. We begin by setting $v_n = 1$ in (9) and differentiate the left side to get,

$$Y_{n+1} = Y_n + \langle f(\mathcal{I}Y), 1 \rangle_{I_n, Q^f} + \langle g(\mathcal{I}Y), 1 \rangle_{I_n, Q^g}. \quad (12)$$

Now applying the quadrature rules and the definition of $\mathcal{I}Y$,

$$\begin{aligned} Y_{n+1} &= Y_n + k_n \sum_{i=1}^{\nu} w_i f(\mathcal{I}^n Y(t_{n+d_i})) + k_n \sum_{i=1}^{\nu} v_i g(\mathcal{I}^n Y(t_{n+d_i})) \\ &= Y_n + k_n \sum_{i=1}^{\nu} w_i f(\tilde{Y}_i) + k_n \sum_{i=1}^{\nu} v_i g(\tilde{Y}_i). \end{aligned} \quad (13)$$

which is the update formula for the IMEX scheme. \square

2.4 Convergence of Equivalent Finite Element Method

We now prove that the above finite element method converges to the exact solution as the mesh is refined. We consider second order or higher methods, as IMEX schemes of interest are generally at least second order. The above equivalency shows that $Y(t)$ interpolates the exact solution $y(t)$ at the nodes t_n to at least second order for such an IMEX scheme, and therefore for sufficiently small k ,

$$|y(t_n) - Y(t_n)| \leq Ck^2, \quad (14)$$

where $k = \max_n k_n$.

The following lemma discusses stability of interpolation to perturbations in the interpolated values.

Lemma 1. *Let $p(t)$ and $\tilde{p}(t)$ interpolate the points $(x_0, v_0), \dots, (x_r, v_r)$ and $(x_0, \tilde{v}_0), \dots, (x_r, \tilde{v}_r)$ respectively with Lagrange polynomial interpolation. If*

$$\max_{x \in [x_0, x_r]} \sum_{i=0}^r |\ell_i(x)| = \Lambda < \infty, \quad (15)$$

where $\ell_i(x)$ are the Lagrange basis functions then

$$\|p - \tilde{p}\|_{\infty, [x_0, x_r]} \leq \Lambda \|\mathbf{v} - \tilde{\mathbf{v}}\|_{\infty}, \quad (16)$$

where $\|\cdot\|_{\infty, [x_0, x_r]}$ is the $L^\infty([x_0, x_r])$ norm, $\|\cdot\|_{\infty}$ is the max norm, $\mathbf{v} = [v_0, \dots, v_r]^T$ and $\tilde{\mathbf{v}} = [\tilde{v}_0, \dots, \tilde{v}_r]^T$

We now show convergence using a cG(1) method.

Theorem 2. *If $Y(t)$ is a cG(1) solution of (9) corresponding to an IMEX scheme of at least second order, then for sufficiently small k ,*

$$\|y(t) - Y(t)\|_{\infty} \leq (C_1 + C)k^2, \quad (17)$$

where C and C_1 are constants independent of k .

Proof. By equivalence shown above we have that

$$|y(t_n) - Y(t_n)| \leq Ck^2 \quad \forall n = 0, \dots, N-1. \quad (18)$$

Let $I(t)$ be the continuous piecewise linear interpolant through the points $(t_n, y(t_n))$. By definition, the restriction of $Y(t)$ to I_n linearly interpolates the values Y_n and Y_{n+1} . Using interpolation theory[27] and Lemma 1 we have,

$$\begin{aligned} \|y - Y\|_{\infty, [0, T]} &= \max_n \|y - Y\|_{\infty, I_n} \\ &\leq \max_n \|y - I\|_{\infty, I_n} + \max_n \|I - Y\|_{\infty, I_n} \\ &\leq C_1 k^2 + \max_n \left\{ \max (|y(t_n) - Y(t_n)|, |y(t_{n+1}) - Y(t_{n+1})|) \right\} \\ &\leq (C_1 + C)k^2, \end{aligned} \quad (19)$$

where the constant $\Lambda = 1$ from Lemma 1, since the linear Lagrange basis functions are positive and sum to unity, and C_1 is a constant from standard interpolation theory. Therefore due to the convergence of the IMEX scheme, the finite element solution also converges. \square

3 A posteriori Analysis

In this section, we derive a posteriori error estimates based on adjoint operators. In particular, we derive estimates for the quantity $(y(T) - Y(T), \psi)$ where the vector ψ defines the QoI, see (2). The a posteriori analysis follows from the equivalence of the Runge-Kutta IMEX scheme (5) with the finite element method (9). Throughout this section, y denotes the solution to the continuum ODE problem (1) whereas Y represents the solution to the finite element method in (9). Theorem 1 and 2 ensure the error analysis of the finite element solution also applies to the Runge-Kutta IMEX solution.

3.1 Adjoint Problem

There is no unique definition for adjoint operators corresponding to nonlinear operators. We employ a definition which is standard for a posteriori analysis [4]. We consider the linearized operator,

$$\overline{H_{y,Y}} = \int_0^1 \frac{df(z)}{dy} + \frac{dg(z)}{dy} ds. \quad (20)$$

where $z = sy + (1-s)Y$. By the chain rule and the Fundamental Theorem of Calculus, this definition implies,

$$\begin{aligned} \overline{H_{y,Y}}(y - Y) &= \int_0^1 \frac{df(z)}{dy} (y - Y) + \frac{dg(z)}{dy} (y - Y) ds \\ &= \int_0^1 \frac{df(z)}{ds} + \frac{dg(z)}{ds} = (f(y) - f(Y)) + (g(y) - g(Y)). \end{aligned} \quad (21)$$

The linearized operator is used to define the adjoint problem for the quantity of interest,

$$\begin{cases} -\dot{\phi} = \overline{H_{y,Y}}^\top \phi, & t \in (T, 0], \\ \phi(T) = \psi. \end{cases} \quad (22)$$

Notice that the adjoint problem is solved “backwards” in time.

3.2 Error Representations

Let $e = y - Y$ be the error and let ξ_n denote the value at time t_n for a function ξ .

Lemma 2 (Error Representation on an Interval). *On each interval I_n we have,*

$$(e_{n+1}, \phi_{n+1}) = (e_n, \phi_n) + \langle f(Y) + g(Y) - \dot{Y}, \phi \rangle_{I_n}. \quad (23)$$

Proof. The proof is standard, e.g. see [28]. \square

Theorem 3 (Error Representation). *If $y(t)$ and $Y(t)$ are solutions of (1) and (9) respectively, and φ is a solution of the adjoint problem (22), then the error in the quantity of interest defined by ψ is given by,*

$$(y(T) - Y(T), \psi) = E1 + E2 + E3, \quad (24)$$

where,

$$E1 = \sum_{n=0}^{N-1} E1_n, \quad E2 = \sum_{n=0}^{N-1} E2_n, \quad E3 = \sum_{n=0}^{N-1} E3_n, \quad (25)$$

and

$$\begin{aligned} E1_n &= \langle -\dot{Y}, \phi - \pi_n \phi \rangle_{I_n} + \langle f(\mathcal{I}Y), \phi - \pi_n \phi \rangle_{I_n, Q^f} + \langle g(\mathcal{I}Y), \phi - \pi_n \phi \rangle_{I_n, Q^g}, \\ E2_n &= \langle f(Y), \phi \rangle_{I_n} - \langle f(\mathcal{I}Y), \phi \rangle_{I_n, Q^f}, \\ E3_n &= \langle g(Y), \phi \rangle_{I_n} - \langle g(\mathcal{I}Y), \phi \rangle_{I_n, Q^g}. \end{aligned} \quad (26)$$

Here $\pi_n \phi$ represents a projection of $\phi|_{I_n}$ onto the space $\mathcal{P}^{q-1}(I_n)$. The terms $E1$, $E2$ and $E3$ represent the discretization, explicit and implicit contributions to the error respectively.

Proof. Adding (23) over all intervals for $n = 0, \dots, N-1$ we have,

$$\sum_{n=0}^{N-1} (e_{n+1}, \phi_{n+1}) = \sum_{n=0}^{N-1} \left[(e_n, \phi_n) + \langle f(Y) + g(Y) - \dot{Y}, \phi \rangle_{I_n} \right]. \quad (27)$$

Now $\sum_{n=0}^{N-1} (e_{n+1}, \phi_{n+1}) = \sum_{n=1}^{N-1} (e_n, \phi_n) + (e_N, \phi_N)$. Using this in (27) along with the fact that the numerical solution satisfies the initial condition, i.e. $e_0 = 0$, we arrive at,

$$(e_N, \phi_N) = \sum_{n=0}^{N-1} \left[\langle f(Y) + g(Y) - \dot{Y}, \phi \rangle_{I_n} \right]. \quad (28)$$

Adding and subtracting $\sum_{n=0}^{N-1} \langle f(\mathcal{I}Y), \phi \rangle_{I_n, Q^f}$ and $\sum_{n=0}^{N-1} \langle g(\mathcal{I}Y), \phi \rangle_{I_n, Q^g}$ to the right hand side of (28) leads to,

$$(e_N, \phi_N) = \sum_{n=0}^{N-1} \left[\langle -\dot{Y}, \phi \rangle_{I_n} + \langle f(\mathcal{I}Y), \phi \rangle_{I_n, Q^f} + \langle g(\mathcal{I}Y), \phi \rangle_{I_n, Q^g} + E2_n + E3_n \right]. \quad (29)$$

Now, since $\pi_n \phi \in \mathcal{P}^{q-1}(I_n)$, we have from (9) for $n = 0, \dots, N-1$,

$$\langle \dot{Y}, \pi_n \phi \rangle_{I_n} - \langle f(\mathcal{I}Y), \pi_n \phi \rangle_{I_n, Q^f} - \langle g(\mathcal{I}Y), \pi_n \phi \rangle_{I_n, Q^g} = 0, \quad (30)$$

Combining (29) and (30) completes the proof. \square

3.3 A posteriori analysis for time dependent quantities-of-interest

The QoI defined in (2) is based only on the final time of the solution. The analysis above is easily modified for other quantities of interest. For example consider the a time dependent QoI,

$$\widehat{QoI} \equiv \int_0^T (y(t), \tilde{\psi}(t)) dt, \quad (31)$$

where the time dependent function, $\tilde{\psi} : \mathbb{R} \rightarrow \mathbb{R}^m$, defines the QoI. Define the adjoint problem as,

$$\begin{cases} -\dot{\tilde{\phi}} = \overline{H_{y,Y}}^\top \tilde{\phi} + \tilde{\psi}, & t \in (T, 0] \\ \tilde{\phi}(T) = 0. \end{cases} \quad (32)$$

Note that this adjoint problem differs from (22) in the initial conditions and data on the right hand side. This leads to the following error representation.

Theorem 4. *If $y(t)$ and $Y(t)$ are solutions of (1) and (9) respectively, and $\tilde{\varphi}$ is a solution of the adjoint problem (32), then the error in the quantity of interest defined by $\tilde{\psi}$ is given by,*

$$\int_0^T (y(t) - Y(t), \tilde{\psi}(t)) = \tilde{E}1 + \tilde{E}2 + \tilde{E}3, \quad (33)$$

where,

$$\begin{aligned} \tilde{E}1 &= \sum_{n=0}^{N-1} \langle -\dot{Y}, \tilde{\phi} - \pi_n \tilde{\phi} \rangle_{I_n} + \langle f(\mathcal{I}Y), \tilde{\phi} - \pi_n \tilde{\phi} \rangle_{I_n, Q^f} + \langle g(\mathcal{I}Y), \tilde{\phi} - \pi_n \tilde{\phi} \rangle_{I_n, Q^g}, \\ \tilde{E}2 &= \sum_{n=0}^{N-1} \langle f(Y), \tilde{\phi} \rangle_{I_n} - \langle f(\mathcal{I}Y), \tilde{\phi} \rangle_{I_n, Q^f}, \\ \tilde{E}3 &= \sum_{n=0}^{N-1} \langle g(Y), \tilde{\phi} \rangle_{I_n} - \langle g(\mathcal{I}Y), \tilde{\phi} \rangle_{I_n, Q^g}. \end{aligned} \quad (34)$$

Proof. The proof is similar to that of Theorem 3. \square

3.4 Extension of the analysis for space-time discretization of PDEs

The primary aim of this article is to quantify the error due to time integration using the IMEX Runge-Kutta schemes. Hence the analysis presented in this article deals with the error in the numerical solution of an ODE system. As mentioned earlier, such ODE systems often arise from spatial discretization of

one-dimensional partial differential equations. In this article, we ignore the error in the solution to the PDE due to this spatial discretization. The extension of the analysis to the case of PDEs to quantify the effect of spatial discretization follows directly from the analysis of ODEs, e.g. see [10, 23] for details.

4 Numerical Experiments

In this section we consider numerical examples for system of ODEs of the form (1) arising from the spatial discretization of PDEs. The spatial derivatives are discretized using a second order central finite difference scheme in space. The spatial discretization parameter is referred to as h . The error representation formulas require formulating and solving the adjoint (22). In theory, the adjoint is obtained by linearizing around a combination of the discrete solution and the true solution. In practice, we linearize around the discrete solution only [4]. Moreover, the adjoint solution needs to be approximated numerically. We approximate the adjoint solution using the cG($q+1$) finite element method where q is degree of polynomial for the forward solution Y in (9). The higher order approximation of the adjoint problem ensures that the error estimates are accurate.

The approximation of the adjoint solution leads to an “error estimate” from the error representation (24). The effectivity ratio measures the accuracy of the estimate and is defined as,

$$\rho_{\text{eff}} = \frac{\text{Estimated error}}{\text{True error}}.$$

An accurate error estimate has an effectivity ratio close to one. In our examples, the true solution is unknown and is approximated to a high degree of accuracy using MATLAB’s ODE solver.

We show results for three IMEX schemes, Midpoint(1,2,2), IMEX-SSP3(3,3,2) and IMEX-SSP3(4,3,3), whose Butcher tableaux are given in Tables 1, 2 and 3. These are labeled as Mid(1,2,2), SSP3(3,3,2) and SSP3(4,3,3) respectively in the results. We present five examples. The first three examples arise from the finite difference discretization of scalar-valued PDEs, all of which were previously considered in [13]. In these examples we chose f to be the term arising from the first-order spatial derivatives, while g represents the term arising from second-order spatial derivatives. In the fourth example we illustrate how the choice of f and g effects the components of the error estimate. The final example is a simplified 1D Magneto-Hydrodynamics problem.

4.1 Linear PDE

Consider the scalar valued linear PDE

$$\begin{cases} \dot{u} + \sin(2\pi x)u_x = \gamma u_{xx}, & (x, t) \in [0, 1] \times (0, T], \\ u(x, 0) = \sin(2\pi x), & x \in [0, 1], \end{cases} \quad (35)$$

with periodic boundary conditions.

We choose the spatial discretization parameter as $h = 1/40$ and the time step as $k_n = 1/10$. We choose the QoI as $\psi = [\mathbf{1} \quad \mathbf{0}]^\top$, where $\mathbf{1}$ is an $(m/2 + 1)$ vector of all ones and $\mathbf{0}$ is an $(m/2 - 1)$ vector of all zeros. QoIs of this form often arise from evaluating spatial integrals of the PDE solution, $u(x, t)$, at the final time, i.e. $C \int_a^b u(x, t) dx$.

The results for $\gamma = 0.1$ and two values of the final time, T , are shown in Tables 4 and 5 respectively. The results indicates that the error estimate is quite accurate for all schemes, as shown by the effectivity ratio. The error estimates are even accurate when the error is quite large, as is seen in Table 5 for the case of the Midpoint(1,2,2) scheme. The large error in this scheme is due to instabilities that develop in the solution, see Figure 1a. The results for $\gamma = 0.01$ are shown in Tables 6 and 7 for $T = 1.0$ and $T = 2.0$ respectively. Once again the error estimates are quite accurate. Moreover, the error estimates indicate instability in the IMEX-SSP3(4,3,3) solution in addition to the Midpoint(1,2,2) solution for $T = 2.0$. This is also seen in the plots of the solutions in Figure 2. This figure indicates that IMEX-SSP3(3,3,2) remains stable whereas the other two schemes develop instabilities after a certain time. The IMEX-SSP3(4,3,3) seems to be more stable than the Midpoint(1,2,2) solution.

| Scheme | Comp. Err. | Eff. Ratio | $E1$ | $E2$ | $E3$ |
|-------------|------------|------------|-----------|-----------|-----------|
| Mid(1,2,2) | -4.53E-03 | 0.99 | -7.43E-02 | 4.26E-02 | 2.72E-02 |
| SSP3(3,3,2) | 1.428E-03 | 0.99 | 3.37E-03 | 6.89E-03 | -8.83E-03 |
| SSP3(4,3,3) | -5.83E-04 | 1.00 | 2.13E-04 | -4.58E-03 | 3.78E-03 |

Table 4: Results for the problem in §4.1 with the final time $T = 1.0$ and $\gamma = 0.1$ using the Midpoint(1,2,2), IMEX-SSP3(3,3,2) and IMEX-SSP3(4,3,3)schemes.

| Scheme | Comp. Err. | Eff. Ratio | $E1$ | $E2$ | $E3$ |
|-------------|------------|------------|-----------|-----------|-----------|
| Mid(1,2,2) | -1.90E+02 | 1.00 | -1.07E+03 | 1.45E+03 | -5.72E+02 |
| SSP3(3,3,2) | 2.68E-06 | 1.00 | 2.62E-05 | 4.64E-05 | -6.99E-05 |
| SSP3(4,3,3) | -1.89E-06 | 0.99 | -6.30E-05 | -1.91E-05 | 8.11E-05 |

Table 5: Results for the problem in §4.1 with the final time $T = 2.0$ and $\gamma = 0.1$ using the Midpoint(1,2,2), IMEX-SSP3(3,3,2) and IMEX-SSP3(4,3,3)schemes.

4.2 Non-linear PDE with explicit terms only

Consider

$$\begin{cases} \dot{u} + \frac{1}{2} \cos(2\pi t)(1 + u)u_x = 0, & (x, t) \in [0, 1] \times (0, T], \\ u(x, 0) = \sin(2\pi x), & x \in [0, 1], \end{cases} \quad (36)$$

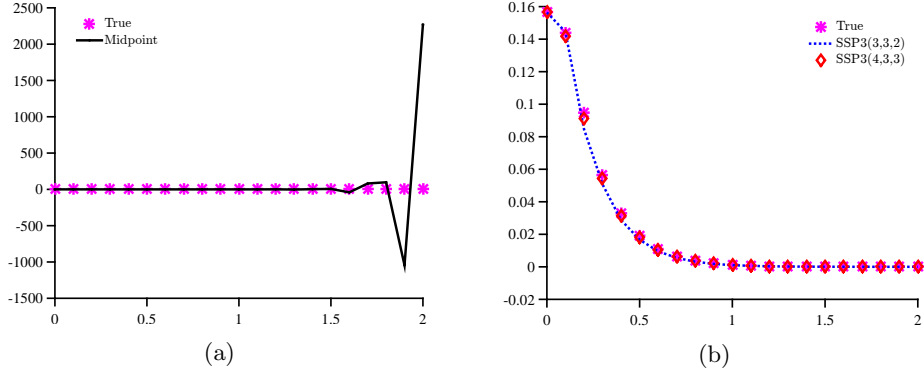


Figure 1: Plot of the $m/2$ th component of the solutions of (35) for $\gamma = 0.1$.

| Scheme | Comp. Err. | Eff. Ratio | $E1$ | $E2$ | $E3$ |
|-------------|------------|------------|----------|----------|-----------|
| Mid(1,2,2) | -1.83E-01 | 0.99 | -2.27E-1 | 9.34E-2 | -4.944E-2 |
| SSP3(3,3,2) | 6.36E-03 | 1.00 | 1.12E-2 | -8.63E-3 | 4.371E-3 |
| SSP3(4,3,3) | 8.51E-04 | 0.99 | -8.72E-3 | 2.33E-3 | 7.24E-3 |

Table 6: Results for the problem in §4.1 with the final time $T = 1.0$ and $\gamma = 0.01$ using the Midpoint(1,2,2), IMEX-SSP3(3,3,2) and IMEX-SSP3(4,3,3)schemes.

| Scheme | Comp. Err. | Eff. Ratio | $E1$ | $E2$ | $E3$ |
|-------------|------------|------------|-----------|-----------|----------|
| Mid(1,2,2) | 3.22E+03 | 1.00 | -1.41E+03 | 3.83E+03 | 8.00E+02 |
| SSP3(3,3,2) | 8.02E-03 | 1.00 | -1.96E-03 | 8.31E-03 | 1.67E-03 |
| SSP3(4,3,3) | -1.46E+00 | 1.00 | -2.24E+00 | -3.28E-01 | 1.10E+00 |

Table 7: Results for the problem in §4.1 with the final time $T = 2.0$ and $\gamma = 0.01$ using the Midpoint(1,2,2), IMEX-SSP3(3,3,2) and IMEX-SSP3(4,3,3)schemes.

with periodic boundary conditions. The QoI is again chosen as $\psi = [\mathbf{1} \quad \mathbf{0}]^T$, where $\mathbf{1}$ is an $(m/2+1)$ vector of all ones and $\mathbf{0}$ is an $(m/2-1)$ vector of all zeros. Here $g(t) \equiv 0$. We choose the spatial discretization parameter as $h = 1/40$ and time step as $k_n = 1/20$. The results for two different values of the final time, T , are shown in Tables 8 and 9. The error estimates are quite accurate with effectivity ratios close to one. Note that the component $III = 0$ as $g = 0$ for this example. The Midpoint(1,2,2) has the lowest error for this example.

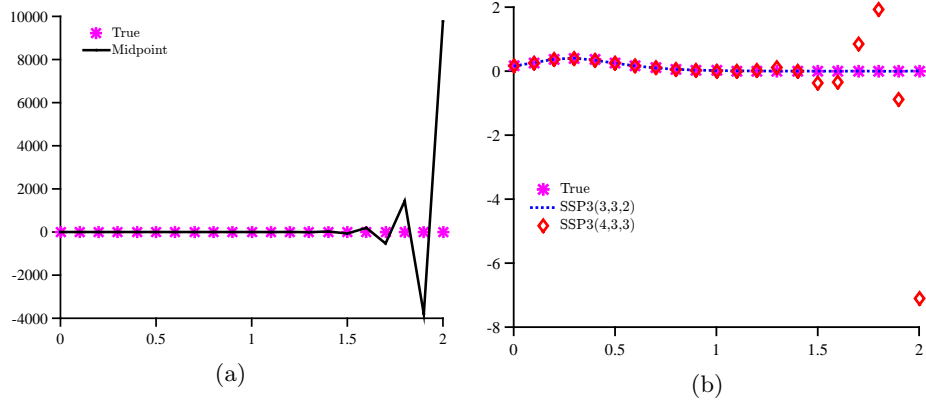


Figure 2: Plot of the $m/2$ th component of the solutions of (35) for $\gamma = 0.01$.

| Scheme | Comp. Err. | Eff. Ratio | $E1$ | $E2$ | $E3$ |
|-------------|------------|------------|-----------|-----------|------|
| Mid(1,2,2) | -5.79E-03 | 1.00 | -2.25E-04 | -5.57E-03 | 0 |
| SSP3(3,3,2) | -2.03E-02 | 0.99 | 1.23E-05 | -2.03E-02 | 0 |
| SSP3(4,3,3) | -3.06E-02 | 0.99 | 4.52E-04 | -3.11E-02 | 0 |

Table 8: Results for the problem in §4.2 with the final time $T = 1.0$ using the Midpoint(1,2,2), IMEX-SSP3(3,3,2) and IMEX-SSP3(4,3,3)schemes..

| Scheme | Comp. Err. | Eff. Ratio | $E1$ | $E2$ | $E3$ |
|-------------|------------|------------|-----------|-----------|------|
| Mid(1,2,2) | -5.96E-03 | 1.04 | -1.08E-03 | -4.87E-03 | 0 |
| SSP3(3,3,2) | -4.10E-02 | 0.99 | 2.61E-05 | -4.11E-02 | 0 |
| SSP3(4,3,3) | -6.19E-02 | 1.00 | 9.74E-04 | -6.29E-02 | 0 |

Table 9: Results for the problem in §4.2 with the final time $T = 2.0$ using the Midpoint(1,2,2), IMEX-SSP3(3,3,2) and IMEX-SSP3(4,3,3)schemes..

4.3 Damped non-linear Burger's equation

The damped non-linear Burger's equation is

$$\begin{cases} \dot{u} + uu_x = \gamma u_{xx}, & (x, t) \in [-1, 1] \times (0, T], \\ u(x, 0) = \sin(\pi x), & x \in [-1, 1], \end{cases} \quad (37)$$

which we consider with periodic boundary conditions. The QoI is again chosen as $\psi = [\mathbf{1} \quad \mathbf{0}]^\top$, where $\mathbf{1}$ is an $(m/2 + 1)$ vector of all ones and $\mathbf{0}$ is an $(m/2 - 1)$ vector of all zeros. We choose the spatial discretization parameter as $h = 1/40$, the time step as $k_n = 1/20$ and $\gamma = 0.05$. The results for two different values of the final time, T , are shown in Tables 10 and 11. The error estimate is again quite accurate, with effectivity ratios close to one. The IMEX-SSP3(4,3,3)

method has the least error for this example.

| Scheme | Comp. Err. | Eff. Ratio | $E1$ | $E2$ | $E3$ |
|-------------|------------|------------|-----------|-----------|-----------|
| Mid(1,2,2) | -8.13E-03 | 1.00 | -1.80E-04 | -1.98E-02 | 1.18E-02 |
| SSP3(3,3,2) | -6.84E-03 | 1.00 | -1.64E-04 | -8.47E-03 | 1.79E-03 |
| SSP3(4,3,3) | -2.30E-04 | 1.00 | 1.04E-05 | 7.14E-04 | -9.55E-04 |

Table 10: Results for the problem in §4.3 with the final time $T = 1.0$ using the Midpoint(1,2,2), IMEX-SSP3(3,3,2) and IMEX-SSP3(4,3,3)schemes..

| Scheme | Comp. Err. | Eff. Ratio | $E1$ | $E2$ | $E3$ |
|-------------|------------|------------|-----------|-----------|-----------|
| Mid(1,2,2) | 1.10E-03 | 0.98 | -7.17E-04 | -4.00E-03 | 5.82E-03 |
| SSP3(3,3,2) | -1.16E-03 | 1.00 | -5.98E-04 | -1.51E-03 | 9.50E-04 |
| SSP3(4,3,3) | 1.35E-04 | 0.99 | 4.20E-06 | 3.59E-04 | -2.28E-04 |

Table 11: Results for the problem in §4.3 with the final time $T = 2.0$ using the Midpoint(1,2,2), IMEX-SSP3(3,3,2) and IMEX-SSP3(4,3,3)schemes.

4.4 Effect of choice of f and g

The choice of f and g is often not obvious for complex problems. In this example, we show how the components of the error estimate capture the effects of the choice of the explicit and implicit parts. To illustrate this, we reverse the choice of f and g in the linear PDE of §4.1. That is, we set f as the term arising from γu_{xx} and g as term arising from $\sin(2\pi x)u_x$. The results for this choice for the same QoI as in §4.1 are shown in Table 12 for $\gamma = 0.075$, $k_n = 1/40$ and $h = 1/20$. We observe that this choice of f and g leads to instability for the Midpoint(1,2,2) scheme, which has a large error relative to the IMEX-SSP schemes. Moreover, we note that the contribution of the component $E2$, which corresponds to the error due to integration of the explicit term, dominates the error estimate and is significantly larger than the other two contributions, $E1$ and $E3$, as expected. These results are in contrast to the results in Tables 4–7, where the component $E2$ is not the dominant term.

4.5 1D Magneto-Hydrodynamic Problem

For our final result, we consider a one-dimensional simplification of three-dimensional Magneto-Hydrodynamic(MHD **is this correct?**) equations. This problem is an analytic asymptotic model for the propagation of an Alfvén wave in a viscous conducting fluid that fills the half space above the x -axis. The solution is of the form $\mathbf{B} = (B, B_0, 0)$ and $\mathbf{v} = (v, 0, 0)$. The model equations are the

| Scheme | Comp. Err. | Eff. Ratio | $E1$ | $E2$ | $E3$ |
|-------------|------------|------------|-----------|-----------|-----------|
| Mid(1,2,2) | 1.75E+06 | 1.00 | 1.16E+05 | 1.64E+06 | 1.27E+04 |
| SSP3(3,3,2) | -4.48E-02 | 1.00 | -6.22E-03 | -3.92E-02 | 6.45E-04 |
| SSP3(4,3,3) | -7.14E-02 | 1.00 | -1.95E-02 | -5.16E-02 | -2.11E-04 |

Table 12: Results for the problem in §4.3 with the final time $T = 1.0$ and an unstable choice of f and g using the Midpoint(1,2,2), IMEX-SSP3(3,3,2) and IMEX-SSP3(4,3,3)schemes.

x -momentum equation with Lorentz forcing term,

$$\frac{\partial v}{\partial t} = \frac{B_0}{\rho} \frac{\partial B}{\partial z} + \frac{\mu}{\rho} \frac{\partial^2 v}{\partial z^2}, \quad (38)$$

and the x -magnetic induction equation,

$$\frac{\partial B}{\partial t} = B_0 \frac{\partial v}{\partial z} + \frac{\eta}{\mu_0} \frac{\partial^2 B}{\partial z^2}. \quad (39)$$

These equations are often used to test more complicated three-dimensional MHD codes, as the 1D counterpart has an analytic solution,

$$v(z, t) = \frac{U}{4} \left[e^{\frac{-A_0 z}{d}} \left(1 - \operatorname{erf} \left(\frac{z - A_0 t}{2\sqrt{dt}} \right) \right) - \operatorname{erf} \left(\frac{z - A_0 t}{2\sqrt{dt}} \right) \right] + \quad (40)$$

$$\frac{1}{4} U \left[e^{\frac{A_0 z}{d}} \left(1 - \operatorname{erf} \left(\frac{z + A_0 t}{2\sqrt{dt}} \right) \right) - \operatorname{erf} \left(\frac{z + A_0 t}{2\sqrt{dt}} \right) + 2 \right],$$

$$B(z, t) = -\frac{1}{4} e^{\frac{-A_0 z}{d}} \left(-1 + e^{\frac{A_0 z}{d}} \right) U \sqrt{\mu \rho} \left[\operatorname{erfc} \left(\frac{z - A_0 t}{2\sqrt{dt}} \right) + e^{\frac{A_0 z}{d}} \operatorname{erfc} \left(\frac{z + A_0 t}{2\sqrt{dt}} \right) \right], \quad (41)$$

where $d = \eta/\mu_0$.

We consider this problem with parameters $B_0 = 10$ with all other parameters are set to 1. The initial conditions are chosen to be $v = B = 0$. Plots of the true solution and IMEX solution for the velocity variable, v , at different times for two IMEX different schemes are shown in Figure 3. For the IMEX solutions, the boundary conditions obtained from the exact solution. We discretize the spatial domain with discretization parameter $h = 5 \times 10^{-3}$ to obtain a system of the form (1), which we solve to final time $T = 0.1$ with time step $k_n = 1 \times 10^{-3}$. The second-order operators were integrated implicitly and the first-order operators (corresponding to the Alfvén wave) were treated explicitly, see § 4.5.1. The figure indicates that the solution for the Midpoint(1,2,2) scheme in Figure 3a is unstable, whereas the solution for the IMEX-SSP3(3,3,2) in Figure 3b scheme is quite accurate. The plot for the IMEX-SSP3(4,3,3) is similar to Figure 3b. The accuracy of the solutions indicated by the figures in also indicated in the error estimates in § 4.5.1.

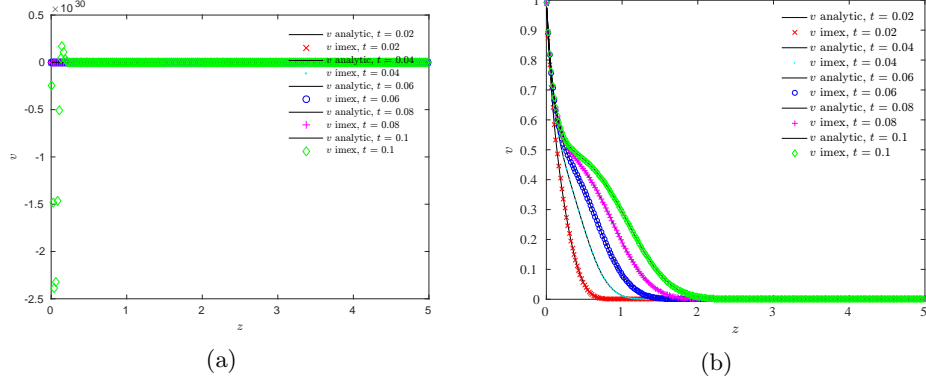


Figure 3: Plot of v for the problem in (38) and (39) at different times. The analytic solution, labeled v analytic, is a solid black line. The IMEX solution is label v imex. (a) Solution obtained using the Midpoint(1,2,2) scheme. (b) Solution obtained using the IMEX-SSP3(3,3,2) scheme. The solution for the midpoint scheme exhibits instabilities whereas the solution for the IMEX-SSP3(3,3,2) scheme is quite accurate. The plot for the IMEX-SSP3(4,3,3) is similar to the one for the IMEX-SSP3(3,3,2) scheme.

We choose a quantity of interest $\int_0^L v dz$ where $z \in [0, L]$ belongs to the spatial domain considered for the problem. We further decompose the solution as $y = [y_v, y_B]^\top$ with the components y_v and y_B corresponding to the (spatially discretized) variables v and B respectively. Similarly, we decompose $f = [f_v, f_B]^\top$, $g = [g_v, g_B]^\top$ and the adjoint solution $\phi = [\phi_v, \phi_B]$. For all runs, f_B corresponds to the spatial discretization of the term $B_0 \frac{\partial v}{\partial z}$ and g_B corresponds to the spatial discretization of the term $\frac{\eta}{\mu_0} \frac{\partial^2 B}{\partial z^2}$, with f_v and g_v defined below for each example.

Finally, we decompose the error components from Theorem 3 as,

$$E1 = E1_v + E1_B, \quad E2 = E2_v + E2_B, \quad E3 = E3_v + E3_B, \quad (42)$$

where,

$$E1_v = \sum_{n=0}^{N-1} \langle -\dot{Y}_v, \phi_v - \pi_n \phi_v \rangle_{I_n} + \langle f_v(\mathcal{I}Y), \phi_v - \pi_n \phi_v \rangle_{I_n, Q^f} + \langle g_v(\mathcal{I}Y), \phi_v - \pi_n \phi_v \rangle_{I_n, Q^g}, \quad (43)$$

$$E2_v = \sum_{n=0}^{N-1} \langle f_v(Y), \phi_v \rangle_{I_n} - \langle f_v(\mathcal{I}Y), \phi_v \rangle_{I_n, Q^f}, \quad (44)$$

$$E3_v = \sum_{n=0}^{N-1} \langle g_v(Y), \phi_v \rangle_{I_n} - \langle g_v(\mathcal{I}Y), \phi_v \rangle_{I_n, Q^g}, \quad (45)$$

where $Y = [Y_v, Y_B]^\top$ is the IMEX solution. The definitions for the error contributions corresponding to the B variables follow in a similar manner.

4.5.1 Implicit and Explicit components for the v equation

For our first result we split the v components of the right hand side into both implicit and explicit parts. We choose f_v to correspond with $\frac{B_0}{\rho} \frac{\partial B}{\partial z}$ and g_v to correspond with $\frac{\mu}{\rho} \frac{\partial^2 v}{\partial z^2}$. The results are shown in Tables 13 and 14. We observe that the error estimate has effectivity ratio close to one, even when the actual error is quite large, as is the case for the Midpoint(1,2,2) scheme. The unstable solution for this scheme is depicted in 3a.

| Scheme | Comp. Err. | Eff. Ratio | $E1$ | $E2$ | $E3$ |
|-------------|------------|------------|------------|-----------|-----------|
| Mid(1,2,2) | 1.73e+27 | 1.00 | 8.01 E+26 | -2.10E+26 | 1.13E+27 |
| SSP3(3,3,2) | -3.30E-02 | 1.00 | -3.033E-05 | 1.59E-01 | -1.92E-01 |
| SSP3(4,3,3) | 5.19E-04 | 1.00 | 1.785E-04 | 8.71E-05 | 2.54E-04 |

Table 13: Results for the problem in §4.5 with the choice of f and g given in 4.5.1 and final time $T = 0.1$ using the Midpoint(1,2,2), IMEX-SSP3(3,3,2) and IMEX-SSP3(4,3,3)schemes.

| Scheme | $E1_v$ | $E1_B$ | $E2_v$ | $E2_B$ | $E3_v$ | $E3_B$ |
|-------------|-----------|-----------|-----------|-----------|-----------|-----------|
| Mid(1,2,2) | 8.07E+26 | -6.04E+24 | -1.93E+26 | -1.70E+25 | 9.51E+26 | 1.87E+26 |
| SSP3(3,3,2) | -2.92E-05 | -1.06E-06 | 2.85E-03 | 1.56E-01 | -1.89E-01 | -3.02E03 |
| SSP3(4,3,3) | 1.73E-04 | 4.91E-06 | 4.90E-05 | 3.80E-05 | 3.76E-04 | -1.22E-04 |

Table 14: Different components of the error contributions corresponding to the results in Table 13.

4.5.2 Implicit components only for the v equation

For the next result we choose all the v components of the right hand side to be handled implicitly, thus setting $f_v = 0$ and letting g_v correspond with $\frac{B_0}{\rho} \frac{\partial B}{\partial z} + \frac{\mu}{\rho} \frac{\partial^2 v}{\partial z^2}$. Tables 15 and 16 show the results, and now we observe that all three schemes are stable. The error estimate is again quite accurate.

5 Conclusions

We present adjoint-based *a posteriori* error estimation for multi-stage Runge-Kutta IMEX schemes. These estimates are achieved by representing the IMEX scheme as a finite element method, which uses particular quadratures to obtain

| Scheme | Comp. Err. | Eff. Ratio | $E1$ | $E2$ | $E3$ |
|-------------|------------|------------|------------|------------|------------|
| Mid(1,2,2) | -4.88E-04 | 1.00 | 3.88E-06 | 3.22E-04 | -8.14E-04 |
| SSP3(3,3,2) | -3.27E-02 | 1.00 | -3.57E-07 | 1.55E-01 | -1.87E-01 |
| SSP3(4,3,3) | 6.7628e-04 | 1.00 | 1.1075e-06 | 2.0620e-04 | 4.6897e-04 |

Table 15: Results for the problem in §4.5 with the choice of f and g given in 4.5.2 and final time $T = 0.1$ using the Midpoint(1,2,2), IMEX-SSP3(3,3,2) and IMEX-SSP3(4,3,3)schemes.

| Scheme | $E1_v$ | $E1_B$ | $E2_v$ | $E2_B$ | $E3_v$ | $E3_B$ |
|-------------|-----------|-----------|--------|----------|-----------|-----------|
| Mid(1,2,2) | 1.38E-05 | -9.97E-06 | 0 | 3.22E-04 | -3.10E-03 | 2.28E-03 |
| SSP3(3,3,2) | 1.03E-06 | -1.39E-06 | 0 | 1.55E-01 | -1.85E-01 | -2.87E-03 |
| SSP3(4,3,3) | -3.89E-06 | 5.00E-06 | 0 | 2.06E-04 | 4.51E-04 | 1.73E-05 |

Table 16: Different components of the error contributions corresponding to the results in Table 15.

nodal equivalence with the IMEX scheme. This provides us with an approximation that equals the IMEX approximation at the nodes, but is defined for the entire temporal domain. We then use this approximation to estimate the error in the IMEX approximation. In addition, our analysis distinguishes between error due to the discretization of the temporal domain, the explicit portion of the scheme and the implicit portion of the scheme. This splitting of the error into different contributions allows us to determine what portion of the method is most responsible for inaccuracy, and can inform the user as to the best course method to reduce the error.

Acknowledgments

J. Chaudhry’s work is supported in part by the Department of Energy (DESC0009324). The authors will also like to thank Prof. Don Estep from Colorado State University for discussing the ideas presented here.

References

- [1] L. Pareschi, G. Russo, Implicit-explicit runge-kutta schemes for stiff systems of differential equations, Recent trends in numerical analysis 3 (2000) 269–289.
- [2] D. Estep, *A posteriori* error bounds and global error control for approximation of ordinary differential equations, SIAM J. Numer. Anal. 32 (1) (1995) 1–48.

- [3] K. Eriksson, D. Estep, P. Hansbo, C. Johnson, Computational Differential Equations, Cambridge University Press, Cambridge, 1996.
- [4] D. J. Estep, M. G. Larson, R. D. Williams, A. M. Society, Estimating the error of numerical solutions of systems of reaction-diffusion equations, American Mathematical Society, 2000.
- [5] M. Ainsworth, T. Oden, *A posteriori* error estimation in finite element analysis, John Wiley-Teubner, 2000.
- [6] W. Bangerth, R. Rannacher, Adaptive Finite Element Methods for Differential Equations, Birkhauser Verlag, 2003.
- [7] T. J. Barth, *A posteriori* Error Estimation and Mesh Adaptivity for Finite Volume and Finite Element Methods, Vol. 41 of Lecture Notes in Computational Science and Engineering, Springer, New York, 2004.
- [8] R. Becker, R. Rannacher, An optimal control approach to *a posteriori* error estimation in finite element methods, Acta Numerica (2001) 1–102.
- [9] M. B. Giles, E. Süli, Adjoint methods for pdes: a posteriori error analysis and postprocessing by duality, Acta Numerica 11 (1) (2002) 145–236.
- [10] J. H. Chaudhry, D. Estep, V. Ginting, J. N. Shadid, S. Tavener, A posteriori error analysis of imex multi-step time integration methods for advection–diffusion–reaction equations, Computer Methods in Applied Mechanics and Engineering 285 (2015) 730–751.
- [11] J. Collins, D. Estep, S. Tavener, A posteriori error estimates for explicit time integration methods, BIT Numerical Mathematics.
- [12] L. Pareschi, G. Russo, Implicit-explicit runge-kutta schemes and applications to hyperbolic systems with relaxation, Journal of Scientific Computing. 25 (112) (2005) 129–154.
- [13] U. M. Ascher, S. J. Ruuth, R. J. Spiteri, Implicit-explicit Runge-Kutta methods for time-dependent partial differential equations, Appl. Numer. Math. 25 (2-3) (1997) 151–167. doi:10.1016/S0168-9274(97)00056-1. URL [http://dx.doi.org/10.1016/S0168-9274\(97\)00056-1](http://dx.doi.org/10.1016/S0168-9274(97)00056-1)
- [14] W. Hundsdorfer, S. J. Ruuth, IMEX extensions of linear multistep methods with general monotonicity and boundedness properties, J. Comput. Phys. 225 (2) (2007) 2016–2042. doi:10.1016/j.jcp.2007.03.003. URL <http://dx.doi.org/10.1016/j.jcp.2007.03.003>
- [15] R. Donat, I. Higueras, A. Martinez-Gavara, On stability issues for IMEX schemes applied to 1D scalar hyperbolic equations with stiff reaction terms, Math. Comp. 276 (2011) 2097–2126.

- [16] Y. Kadioglu, D. A. Knoll, R. B. Lowrie, R. M. Rauenzhan, A second order self-consistent IMEX method for radiation hydrodynamics, *J. Comp. Phys.* 229.
- [17] S. Y. Kadioglu, D. A. Knoll, A fully second order implicit/explicit time integration technique for hydrodynamics plus nonlinear heat conduction problems, *J. Comp. Phys.* 229 (2010) 3237–3249.
- [18] M. Svard, S. Mishra, Implicit-explicit schemes for flow equations with stiff source terms, *J. Comp. and Applied Math.* 235 (2011) 1564–1577.
- [19] S. R. Lau, G. Lovelace, H. P. Pfeiffer, Implicit-explicit evolution of single black holes, *Physical Review D.* 84 (2011) 084023.
- [20] C. Roedig, O. Zanotti, D. Alic, General relativistic radiation hydrodynamics of accretion flows - ii. treating stiff source terms and exploring physical limitations, *Mon. Notes Royal Astron. Soc.* 426 (2012) 1613–1631.
- [21] U. M. Ascher, S. J. Ruuth, B. T. R. Wetton, Implicit-explicit methods for time-dependent partial differential equations, *SIAM Journal on Numerical Analysis* 32 (3) (1995) pp. 797–823.
URL <http://www.jstor.org/stable/2158449>
- [22] M. H. Carpenter, C. A. Kennedy, H. Bijl, S. A. Viken, V. N. Vatsa, Fourth-order runge-kutta schemes for fluid mechanics applications, *Journal of Scientific Computing* 25 (112) (2005) 157–194.
- [23] J. Collins, D. Estep, S. Tavener, A posteriori error estimation for the lax-wendroff finite difference scheme, *Journal of Computational and Applied Mathematics* 263 (2014) 299–311.
- [24] T. J. Barth, Space-time error representation and estimation in navier-stokes calculations, in: *Complex Effects in Large Eddy Simulations*, Springer, 2007, pp. 29–48.
- [25] T. J. Barth, M. G. Larson, A posteriori error estimates for higher order godunov finite volume methods on unstructured meshes, *Finite Volumes for Complex Applications III*, London.
- [26] M. G. Larson, T. J. Barth, A posteriori error estimation for adaptive discontinuous galerkin approximations of hyperbolic systems, in: *Discontinuous Galerkin Methods*, Springer, 2000, pp. 363–368.
- [27] S. C. Brenner, R. Scott, *The mathematical theory of finite element methods*, Vol. 15, Springer Science & Business Media, 2008.
- [28] K. Eriksson, D. Estep, P. Hansbo, C. Johnson, Introduction to adaptive methods for differential equations, in: *Acta Numerica*, 1995, *Acta Numerica*, Cambridge Univ. Press, Cambridge, 1995, pp. 105–158.